Giant Ambipolar Rashba Effect in the Semiconductor BiTeI

A. Crepaldi,[1] L. Moreschini,[2] G. Autès,[3] C. Tournier-Colletta,[1] S. Moser,[1] N. Virk,[3] H. Berger,[1] Ph. Bugnon,[1]
Y. J. Chang,[2,4] K. Kern,[1,5] A. Bostwick,[2] E. Rotenberg,[2] O. V. Yazyev,[3] and M. Grioni[1]

[1]*Institute of Condensed Matter Physics, Ecole Polytechnique Fédérale de Lausanne (EPFL), CH-1015 Lausanne, Switzerland*
[2]*Advanced Light Source (ALS), Lawrence Berkeley National Laboratory, Berkeley, California 94720, USA*
[3]*Institute of Theoretical Physics, Ecole Polytechnique Fédérale de Lausanne (EPFL), CH-1015 Lausanne, Switzerland*
[4]*Department of Physics, University of Seoul, Seoul 130-743, Korea*
[5]*Max-Plank-Institut für Festkörperforschung, D-70569, Stuttgart, Germany*
(Received 4 May 2012; published 30 August 2012)

We observe a giant spin-orbit splitting in the bulk and surface states of the noncentrosymmetric
semiconductor BiTeI. We show that the Fermi level can be placed in the valence or in the conduction band
by controlling the surface termination. In both cases, it intersects spin-polarized bands, in the correspond-
ing surface depletion and accumulation layers. The momentum splitting of these bands is not affected by
adsorbate-induced changes in the surface potential. These findings demonstrate that two properties crucial
for enabling semiconductor-based spin electronics—a large, robust spin splitting and ambipolar conduc-
tion—are present in this material.

The relativistic spin-orbit interaction (SOI) lifts the
usual Kramers spin degeneracy in electron systems that
lack inversion symmetry. It lies at the origin of many subtle
and interesting effects in the electronic structure of mate-
rials such as the emergence of topological insulators, a new
quantum state of matter. In the bulk of materials with
noncentrosymmetric structures, such as the zinc blende
and wurzite structures, it gives rise to the Dresselhaus [1]
and Rashba [2] effects. An analogous effect, the Rashba-
Bychkov effect, describes the lifting of the spin degeneracy
at surfaces and at asymmetric interfaces, where inversion
symmetry is also broken [3]. The SOI is a general phe-
nomenon, but it is especially relevant in solids containing
high-Z elements because of their large atomic spin-orbit
parameter. The characteristic splitting in energy and mo-
mentum was first directly observed by angle-resolved
photoelectron spectroscopy (ARPES) on the Au(111) sur-
face [4]. The predicted polarization of the electronic states
was confirmed by spin-polarized ARPES [5,6], and the
Rashba scenario has been extended to other surfaces and
interfaces [7–15].

The vision of an all-electric control of spin transport in
new device concepts explains the strong current interest for
materials with large Rashba or Dresselhaus effects. Future
devices operating at room temperature will require a large
separation between the spin-polarized bands and the ability
to tune the position of the chemical potential over a broad
energy range. Whereas the former have been reported in
surface alloys with high-Z elements such as Pb or Bi, only
limited tunability has been achieved so far.

BiTeI is a noncentrosymmetric semiconductor for which
theory predicts a large bulk Rashba effect, and the emer-
gence of a topological insulating phase under pressure
[16]. Ishizaka *et al.* [17] used spin-resolved ARPES to

reveal spin-polarized states with a large momentum split-
ting. They assigned them to a quantum-well state (QWS)
confined in the accumulation layer that appears because of
band bending in the surface region. This interpretation has
been questioned in part by more recent ARPES data and
calculations that show the coexistence of surface and bulk
bands near the Fermi level [18].

In this Letter, we show that in BiTeI the chemical
potential can be moved well into the conduction band or
the valence band by controlling the surface termination.
Remarkably, a giant spin splitting at the Fermi surface is
observed in both cases. First-principles relativistic calcu-
lations indicate that both the surface and the bulk bands are
split by the SOI. We also prove that the size of the Rashba
effect is largely insensitive to changes in the surface
potential. Therefore, the splitting has mainly an atomic
origin. These results establish BiTeI as a versatile material,
characterized by the coexistence of very large ambipolar
bulk and surface Rashba effects.

We performed ARPES experiments at the Electronic
Structure Factory, beam line 7.0.1 of the Advanced Light
Source. The energy and momentum resolution of the hemi-
spherical Scienta R4000 analyzer were 30 meV and 0.1°.
High quality single crystals of BiTeI, in the form of plate-
lets, were grown by chemical vapor transport and by the
Bridgman technique, and characterized by x-ray diffrac-
tion and transport. They showed a metallic conduction due
to a small ($< 2\%$) deviation from stoichiometry. The
samples were mounted on a He cryostat and cleaved in
UHV to expose flat, shiny surfaces.

First-principles electronic structure calculations were
performed within the density functional theory framework
employing the generalized gradient approximation as
implemented in the QUANTUM-ESPRESSO package [19].

Spin-orbit effects were accounted for using the fully relativistic norm-conserving pseudopotentials acting on valence electron wave functions represented in the two-component spinor form [20]. The surface band structures were obtained using a slab model consisting of 39 atomic layers. Since the BiTeI crystal has no inversion symmetry, the surfaces of the slab are necessarily different. The slab model considered here includes two unpassivated experimentally relevant terminations (Te and I). The surface bands at the two different surfaces were disentangled by projecting the Kohn-Sham wave functions onto atomic wave functions at the surface layer. The bulk and the slab band structures were aligned by matching the potential in the middle of the slab with the bulk potential.

BiTeI has a trigonal layered structure, with Bi, Te, and I planes alternating along the c axis. The Bi and Te planes are covalently bonded to form a positively charged $(BiTe)^+$ bilayer. The ionic coupling between the bilayer and the adjacent I^- plane defines the natural cleavage plane [21]. The topmost layer—Te or I—is identified by the relative intensities of the Te and I $4d$ core levels, as in Fig. 1(a). Ideally, due to the lack of inversion symmetry, the surface termination is uniquely determined by the direction of the c axis. However, repeated cleaves of the same crystal randomly expose both terminations due to the occurrence of stacking faults, which also explains the observation of sixfold symmetry in the Laue patterns (not shown). We have measured "pure" surfaces and also "mixed" surfaces that presented areas with both terminations [22]. Data for the former are illustrated in Fig. 1. The surface charges—positive for Te, negative for I—induce

band bending in opposite directions for the two terminations. The Fermi level lies into either the conduction or the valence band, giving rise to a charge accumulation or, respectively, depletion layer. This is schematically illustrated in Fig. 1(b) and 1(c) and substantiated by the ARPES data. It should be noted that our density functional theory calculations reproduce qualitatively the observed band bending. The surface bands of the Te(I)-terminated surface appear below (above) the bulk conduction (valence) bands [Fig. 1(e) and 1(g)].

Figure 1(d) illustrates the ARPES dispersion of the Te-terminated surface, measured along the $\overline{\Gamma K}$ high-symmetry direction ($\overline{\Gamma K} = 0.96$ Å^{-1}) of the Brillouin zone. The most prominent feature is the split parabolic band (SS_{Te}) straddling the Fermi level E_F. The two subbands have minima at -0.32 eV and are offset by ± 0.055 Å^{-1} around $\bar{\Gamma}$. This is consistent with previous data, and with a Rashba interaction 1 order of magnitude stronger than for the Au (111) benchmark case [17]. This feature is well reproduced in the first-principles band structure of Fig. 1(e). It shows that the spin-split state is localized in the topmost bilayer, and partially overlaps with conduction band states that exhibit a smaller momentum offset. The bulk signal is too weak to be identified in Fig. 1(d), but it can be discerned between SS_{Te} and E_F at closer inspection [22]. The projected bulk valence band exhibits gaps supporting other surface states. These states exhibit an even larger splitting. Their spin polarization has non negligible radial and out-of-plane components [22], at variance with the simple Rashba scenario, and similar to recent observations on topological insulators [23]. The complex manifold cannot
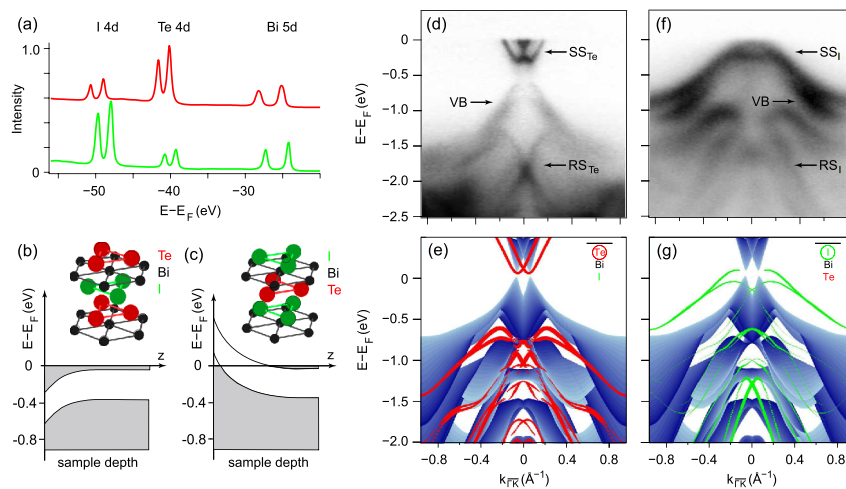

FIG. 1 (color online). (a) I $4d$, Te $4d$, and Bi $5d$ core level spectra measured at $h\nu = 120$ eV on Te- (red, top) and I-terminated (green, bottom) surfaces. (b),(c) Schemes of surface band bending for the two surface terminations. The thickness of the accumulation layer was estimated to be ~ 3 nm in Ref. [17]. (d) ARPES dispersion along the $\overline{\Gamma K}$ direction measured at 93 eV and $T = 40$ K, for a Te-terminated surface, compared to (e) the projected slab band structure calculated from first principles. The size of the red (grey) symbols is proportional to the magnitude of projection onto the surface Te atoms indicated in the inset. The continuum of bulk states is shown in blue. (f),(g) Corresponding plots for the I-terminated surface. The size of the green (grey) symbols in (g) is proportional to the contribution of the surface I atoms indicated in the inset. In (e) and (g) only projection amplitudes larger than 0.1 are shown.

be easily disentangled in the ARPES map, which shows a prominent state, labeled RS_{Te}, symmetrically split around $\bar{\Gamma}$. The maxima of RS_{Te} are at ± 0.2 Å^{-1} and -1.3 eV, corresponding to a very large and previously unnoticed momentum splitting. The bulk valence band (VB), with a maximum 0.37 eV below the bottom of SS_{Te} also exhibits a large spin-orbit splitting, reproduced by the calculation.

The picture from the I-terminated surface [Figs. 1(f) and 1(g)] is quite different. The electron pockets around $\bar{\Gamma}$ are replaced by hole pockets from a spin-split state (SS_I) with a strong projection on the surface I atoms. The momentum offset is again quite large, of the order of ± 0.2 Å^{-1}. A precise determination is difficult because the top of the band lies above E_F. The top of VB is also located above E_F. There is a complete change from electron to hole carriers with respect to Fig. 1(d), which demonstrates ambipolar conduction in BiTeI. The total change in band bending between the Te- and I-terminated surfaces, estimated from core level spectra [22], is $\Delta E_{BB} = 0.9$ eV, to be compared with the estimated energy gap $\Delta E_g \sim 0.38$ eV [17]. Additional features (RS_I) symmetrically split around $\bar{\Gamma}$, can again be identified at higher energy in the ARPES map.

We stress the importance of the ambipolar nature of the low-energy states in view of possible applications. Achieving control of the Fermi level position in Rashba systems or topological insulators has proved a challenging task. Previous strategies based on surface doping by chemi- or physisorbed species, or on alloying, have obvious drawbacks. The former faces the problem of chemical stability, the latter that of disorder leading to a reduced mobility. By contrast, switching between electron and hole conduction is achieved in BiTeI without modifying the ideal crystal structure or the stoichiometry.

The assignment of the spectral features of Fig. 1 to surface or bulk states is further supported by the data shown in Fig. 2(a). It illustrates the photoelectron intensity measured at near-normal emission from a Te-terminated surface as a function of k_z, the wave vector along the c axis. SS_{Te} exhibits an intensity modulation but no dispersion, as expected for true surface states. By contrast, state VB exhibits a ~ 0.7 eV dispersion along $\overline{\Gamma A}$, consistent with its bulk character, and well reproduced by the calculation (dashed line). This is confirmed by constant energy maps (CEM) of these states. The CEM measured at E_F for SS_{Te} [Fig. 2(b)] has two concentric contours typical of the Rashba scenario. The external contour, warped by the interaction with the lattice potential, has a sixfold symmetry, as required by time-reversal symmetry for a surface state [24]. In the CEM measured at the crossing point of RS_{Te} [Fig. 2(d)], the inner contour has collapsed to a point at $\bar{\Gamma}$. The outer contour again exhibits a sixfold symmetry. Interestingly, it is not closed around $\bar{\Gamma}$, but it is broken into 6 disconnected pockets aligned along the 6 equivalent $\overline{\Gamma M}$ directions. This can be seen as the limit of strong warping,
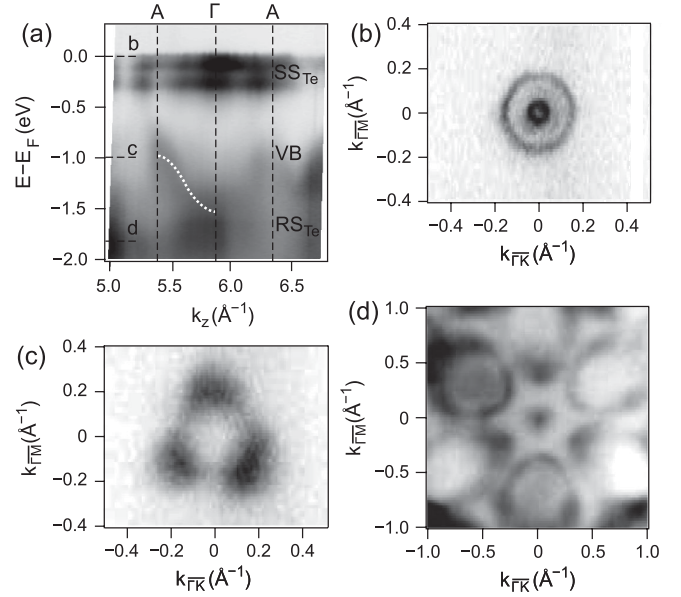

FIG. 2. (a) ARPES intensity from a Te-terminated surface, measured at $\sim 0.3°$ off normal emission, in a photon energy scan between 84 and 162 eV, plotted as a function of k_z, the wave vector along the c axis. Both the upper and the lower branch of SS_{Te} are visible. The white dashed curve is the calculated dispersion of the corresponding bulk valence state. (b)–(d) Constant energy contours measured at the energies marked by the corresponding horizontal lines in panel (a).

reflecting a large in-plane asymmetry of the surface potential [25]. Conversely, the CEM through VB [Fig. 2(c)] shows a single threefold contour. This symmetry reduction is not due to partial extinction of a sixfold contour induced by ARPES matrix elements, because the pattern remained locked to the crystallographic directions when the crystal was rotated around the surface normal. Therefore, the threefold pattern of VB reflects the threefold symmetry of the bulk potential, and confirms the bulk character of this state [22].

We now turn our attention to the origin of the very large Rashba splitting. Competing models beyond the standard Rashba scenario have been proposed. They alternatively stress atomic contributions [26], the in-plane anisotropy of the surface potential [27], the asymmetry of the wave functions [28], or the local orbital angular momentum [29]. A bulk origin has been invoked for BiTeI [17], but this conflicts with the surface nature of the relevant states.

In the standard Rashba scenario, the size of the splitting is controlled by the gradient of the surface potential, and this prediction was found to be consistent with the properties of QWS formed in an accumulation layer at the surface of the topological insulators Bi_2Se_3 [30]. In order to test this hypothesis for BiTeI, we have changed, in a controlled way, the surface band bending, and hence the gradient of the potential in the surface region. This was achieved by depositing increasing amounts of potassium on a Te-terminated surface. Adsorbed K atoms donate
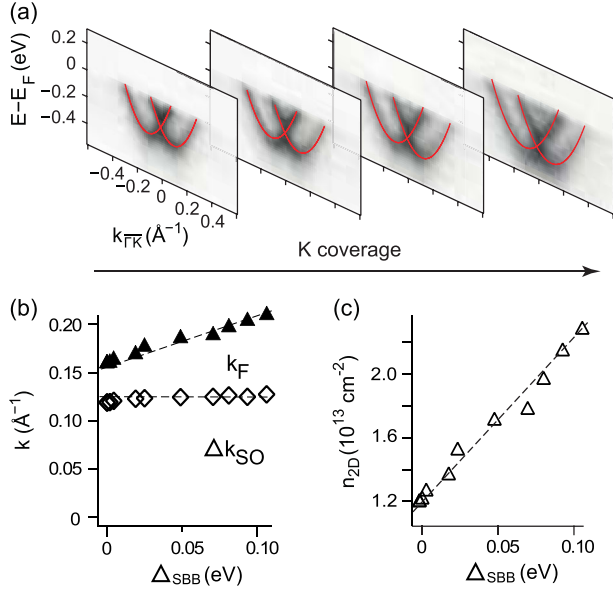
FIG. 3 (color online). (a) Evolution of the spin-split SS_{Te} surface state band as a function of K coverage. The two parabolas are the result of a fit to the band dispersion along $\overline{\Gamma K}$. (b) The Fermi wave vector k_F of the outer branch (solid symbols) and the Rashba splitting Δk_{SO} (empty symbols) are plotted as a function of the measured change in surface band bending Δ_{SBB}. (c) The corresponding surface electron density.

electrons to the conduction band, leaving a positively charged surface layer which enhances the downward surface band bending. Figure 3(a) illustrates the evolution of SS_{Te} as a function of K coverage. Movies of complete K dosing experiments for both Te- and I-terminated surfaces are available in [22].

As expected, SS_{Te} and all core levels [22] shift to lower energies, following the change in band bending. The total shift at saturation K coverage is 0.12 eV, bringing the bottom of SS_{Te} 0.44 eV below E_F. A closer inspection shows that the energy shift of SS_{Te} is rigid. Figure 3(b) shows the Fermi wave vector k_F of the outer branch and the momentum offset Δk_{SO}. They were estimated from a parabolic fit of the dispersion, keeping the effective mass unchanged. Within error bars Δk_{SO} remains constant. The bottom of SS_{Te} gives an upper limit for band bending. Therefore, a $>40\%$ change in the surface band bending has no measurable effect on the strength of the Rashba effect. The SO-split surface state at the Ir(111) surface covered by graphene was recently found to be similarly insensitive to the surface potential gradient [31]. This experimental observation strongly suggests that other parameters, namely, the atomic spin-orbit parameter of the heavy elements, determine the large spin splitting. Figure 3(c) shows that the surface carrier density, estimated from the area of the electron pockets, varies linearly with the downward shift of the split bands. This is again consistent with a constant Δk_{SO}. By contrast, deviations from linearity have been observed for the QWS at the Bi_2Se_3 surface [30].

In summary, we have shown that large ambipolar bulk and surface Rashba effects coexist in the noncentrosymmetric semiconductor BiTeI. The Fermi level at the surface lies either into the valence or the conduction band, depending on the nature of the topmost layer. Achieving ambipolar conduction in a semiconductor with a large Rashba splitting is an important step toward practical applications. In our bulk crystals, the surface termination was randomly chosen by cleavage due to stacking faults, but a definite improvement is possible in thin film samples. Molecular beam epitaxy and chemical vapor deposition—a technique compatible with large-scale thin film production—can in fact be exploited to gain control on the nature of the topmost layer. It is therefore realistic to consider that regions with opposite band bending—a "Rashba *p-n* junction"— could be patterned on a substrate, opening new perspectives for the manipulation of spin-polarized states.

[1] G. Dresselhaus, Phys. Rev. **100**, 580 (1955).
[2] E. I. Rashba, Sov. Phys. Solid State **2**, 1109 (1960).
[3] Y. A. Bychkov and E. I. Rashba, JETP Lett. **39**, 78 (1984).
[4] S. LaShell, B. A. McDougall, and E. Jensen, Phys. Rev. Lett. **77**, 3419 (1996).
[5] M. Hochstrasser, J. G. Tobin, E. Rotenberg, and S. D. Kevan, Phys. Rev. Lett. **89**, 216802 (2002).
[6] M. Hoesch, M. Muntwiler, V. N. Petrov, M. Hengsberger, L. Patthey, M. Shi, M. Falub, T. Greber, and J. Osterwalder, Phys. Rev. B **69**, 241401(R) (2004).
[7] E. Rotenberg, J. W. Chung, and S. D. Kevan, Phys. Rev. Lett. **82**, 4066 (1999).
[8] Y. M. Koroteev, G. Bihlmayer, J. E. Gayone, E. Chulkov, S. Blügel, P. M. Echenique, and P. Hofmann, Phys. Rev. Lett. **93**, 046403 (2004).
[9] O. Krupin, G. Bihlmayer, K. Starke, S. Gorovikov, J. E. Prieto, K. Döbrich, S. Blügel, and G. Kaindl, Phys. Rev. B **71**, 201403(R) (2005).
[10] H. Cercellier, C. Didiot, Y. Fagot-Revurat, B. Kierren, L. Moreau, D. Malterre, and F. Reinert, Phys. Rev. B **73**, 195413 (2006).
[11] I. Barke, F. Zheng, T. K. Rügheimer, and F. J. Himpsel, Phys. Rev. Lett. **97**, 226405 (2006).
[12] C. R. Ast, J. Henk, A. Ernst, L. Moreschini, M. C. Falub, D. Pacilé, P. Bruno, K. Kern, and M. Grioni, Phys. Rev. Lett. **98**, 186807 (2007).

[13] K. He, T. Hirahara, T. Okuda, S. Hasegawa, A. Kakizaki, and I. Matsuda, Phys. Rev. Lett. **101**, 107604 (2008).

[14] K. Sakamoto *et al.*, Phys. Rev. Lett. **103**, 156801 (2009).

[15] I. Gierz, T. Suzuki, E. Frantzeskakis, S. Pons, S. Ostanin, A. Ernst, J. Henk, M. Grioni, K. Kern, and C. R. Ast, Phys. Rev. Lett. **103**, 046803 (2009).

[16] M. S. Bahramy, B.-J. Yang, R. Arita, and N. Nagaosa, Nature Commun. **3**, 679 (2012).

[17] K. Ishizaka, M. S. Bahramy, H. Murakawa, M. Sakano, T. Shimojima, T. Sonobe, K. Koizumi, S. Shin, H. Miyahara, A. Kimura *et al.*, Nature Mater. **10**, 521 (2011).

[18] G. L. Landolt *et al.*, arXiv:1204.2196v1 [Phys. Rev. Lett. (to be published)].

[19] P. Giannozzi, S. Baroni, N. Bonini, M. Calandra, R. Car, C. Cavazzoni, D. Ceresoli, G. L. Chiarotti, M. Cococcioni, I. Dabo *et al.*, J. Phys. Condens. Matter **21**, 395502 (2009).

[20] A. Dal Corso and A. Mosca Conte, Phys. Rev. B **71**, 115106 (2005).

[21] A. V. Shevelkov, E. V. Dikarev, R. V. Shpanchenko, and B. A. Popovkinn, J. Solid State Chem. **114**, 379 (1995).

[22] See Supplemental Material at http://link.aps.org/supplemental/10.1103/PhysRevLett.109.096803 for a detailed characterization of the two surfaces, movies of K adsorption, and for the calculated spin polarization.

[23] S.-Y. Xu, Y. Xia, L. Wray, S. Jia, F. Meier, J. Dil, J. Osterwalder, B. Slomski, A. Bansil, H. Lin *et al.*, Science **332**, 560 (2011).

[24] L. Fu, Phys. Rev. Lett. **103**, 266801 (2009).

[25] E. Frantzeskakis and M. Grioni, Phys. Rev. B **84**, 155453 (2011).

[26] L. Petersen and P. Hedegård, Surf. Sci. **459**, 49 (2000).

[27] J. Premper, M. Trautmann, J. Henk, and P. Bruno, Phys. Rev. B **76**, 073310 (2007).

[28] G. Bihlmayer, S. Blügel, and E. V. Chulkov, Phys. Rev. B **75**, 195414 (2007).

[29] S. R. Park, C. H. Kim, J. Yu, C. Kim, and J. H. Han, Phys. Rev. Lett. **107**, 156803 (2011).

[30] P. D. C. King, R. C. Hatch, M. Bianchi, R. Ovsyannikov, C. Lupulescu, G. Landolt, B. Slomski, J. H. Dil, D. Guan, J. L. Mi *et al.*, Phys. Rev. Lett. **107**, 096802 (2011).

[31] A. Varykhalov, D. Marchenko, M. R. Scholz, E. D. L. Rienks, T. M. Kim, G. Bihlmayer, J. Sanchez-Barriga, and O. Rader, Phys. Rev. Lett. **108**, 066804 (2012).